DEVELOPMENT OF A PREDICTIVE MODEL FOR THE PRELIMINARY DESIGN OF HEAT EXCHANGERS IN ELECTRIC AVIATION

S. Bhapkar, S. Kazula,
German Aerospace Center (DLR), Institute of Electrified Aero Engines,
Lieberoser Str. 13A, 03046 Cottbus, Germany

Abstract

Fuel cells are a promising and viable solution for electrified aircraft engines, offering high energy efficiency and environmental benefits. Carbon-free sustainable aviation fuels such as hydrogen can be used in fuel cells, which convert their chemical energy into electricity, thus reducing the aircraft's emission footprint. A byproduct is heat, which must be effectively removed. It is an engineering challenge to design and implement a heat rejection system suitable for optimized performance, high reliability, and life cycle, while minimizing its weight and drag. Meeting this challenge requires the efficient integration of heat exchangers into the fuel cell-powered aircraft engines.

This paper presents an approach to heat exchange design using a genetic optimization algorithm based on the Python programming language. This algorithm calculates the minimum volume required for the heat exchanger, taking into account the desired pressure drop and heat flow conditions. The accuracy and reliability of the calculations are improved by incorporating the experimental results from the literature and the 3D geometry of heat exchangers, such as offset strip fins. The successful validation of the proposed algorithm highlights its potential for significant time savings during the preliminary design phase of the heat exchangers. Moreover, the genetic optimization algorithm offers a promising solution for achieving optimal heat exchanger performance, minimizing weight and drag, and thereby enhancing overall aircraft efficiency.

Keywords

Heat exchanger, Genetic optimization algorithm, Preliminary design method, Electrified aero engines

1 INTRODUCTION

The future trajectory of aviation is being charted through strategic initiatives such as the European Union's Flightpath 2050 and the Air Transport Action Group's Waypoint 2050 [1], the latter being a manifestation of the commercial aviation industry's own aspirations. The central thrust of these visionary pursuits revolves around curtailing the aviation sector's ecological footprint, with a particular focus on mitigating its role in climate perturbations. The main goals of these efforts are to significantly reduce pollution from nitrogen oxides (NO_x) by more than 90%, cut down carbon dioxide (CO_2) emissions by over 75%, and lower noise from commercial aircraft by more than 65% by the year 2050 [2]. These emission reduction benchmarks are postulated to be within the realm of feasibility through a progressive transition, prominently characterized by the propulsion system's electrification trajectory and the uptake of sustainable aviation fuels that bear a carbon-neutral footprint.

Fuel cells have emerged as a promising technology for powering electrified aero engines due to their high energy efficiency and environmental benefits [3]. In general, a fuel cell (FC) is an electrochemical cell in which electrical energy is converted from the chemical potential of the fuel by encouraging a pair of redox reactions, a reduction and an oxidation reaction. In order to eliminate CO_2 emissions, the fuel of choice ought to be hydrogen H_2, even though other hydrocarbon fuels can be consumed by certain types of fuel cells [3]. Solid oxide fuel cells (SOFCs) are one of the viable options for hydrogen fuel cells. The main advantage of these fuel cells is that they operate at a very high efficiency of 60 to 65 % at the cell level [3]. Due to the high operating temperature, the implementation of fuel cells in electrified aero engines presents challenges, particularly in efficient management of the waste heat generated during their operation [4]. In contrast to gas turbines, where heat is harnessed to enhance air's energy state, generating thrust through impulse energy conversion, fuel cell-generated heat is considered "waste heat" that cannot be similarly utilized for thrust generation and must be expelled from the engine system. It can affect the performance, reliability, and lifecycle of the fuel cell system. Proper dissipation of this waste heat becomes crucial for maintaining optimal operating temperatures and ensuring the safe and efficient aircraft operation. Furthermore, integrating fuel cells in electrified aero engines introduces considerations related to aircraft weight, drag, and overall performance. To efficiently dissipate a substantial amount of heat, such as achieving 50% efficiency where 50% of the input energy is converted into 1MW of electric power (equivalent to 1MW of heat generated), a comprehensive heat rejection system is essential. This system consists of large and heavy components like compressors, heat exchangers, humidifiers, air ducts, and nozzles, all of which must be carefully designed and integrated. Such system impacts weight and drag characteristics of the aircraft. Designing effective heat rejection systems that minimize these adverse effects is essential for the successful integration of fuel cell technology in aeronautical applications [4].

To overcome the challenges associated with developing a waste heat rejection system for fuel cell application, the design and sizing of a compact lightweight heat exchanger becomes imperative. Compact heat exchangers [5] offer the potential for efficient heat transfer while minimizing the

doi: 10.25967/610378

impact on the aircraft's weight and drag. By focusing on innovative heat rejection strategies and compact heat exchanger designs, the efficiency and reliability of electrified aero engines powered by fuel cells can be significantly improved.

The design development of a heat exchanger follows general system engineering steps. Its design fidelity is increased from the conceptual, preliminary and towards the detailed phases. Each stage is accompanied by several assessments to improve the designs and trade studies to down select the best fit solution. The main objective of this paper is to introduce the design and sizing methodology for the preliminary design of the heat exchanger by combining the genetic optimization algorithm [6–8] with geometry-based empirical data [5].

The following paper is structured into several sections. In Chapter 2 Methodology, work flow of the preliminary design is explained in which selection of heat exchanger's material and type is justified. Chapter 2.4 describes the aero-thermal characteristics of a heat exchanger in dependence of different boundary conditions. In Chapter 2.5 different approaches for designing a heat exchanger is explained and reviewed. In subsequence chapter 3, core-mass-velocity approach for heat exchanger design is applied. A multi-objective optimization is described and its implication in trade-offs between HEX size and its aero-thermal performance parameter is made. The results section includes the validation of the optimization and the obtained Pareto fronts for conflicting objectives. Additionally, sensitivity studies on optimization parameters to evaluate their impact are conducted.

2 METHODOLOGY

The process diagram for the preliminary design is shown in FIG 1. This paper introduces a design approach as a preliminary design tool for highly efficient compact heat exchangers. As shown below, first selection of a suitable material for heat exchanger in a waste heat rejection system for a SOFC system is justified. Then, different types of compact heat exchangers are described in short and an adequate type is chosen before proceeding with its design. Selection of a design methodology is justified and the required aero-thermodynamic constraints are explained. Using these input, geometry of the heat exchanger is optimized for the objective of minimum volume, structural mass and frontal areas. Following sections deal with these steps in detail.

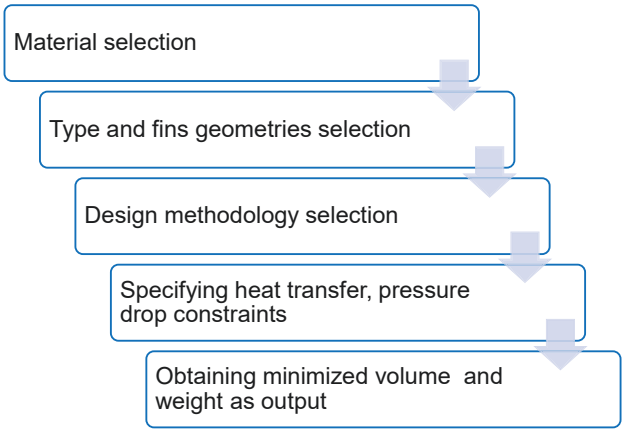

FIG 1. Process diagram for preliminary design.

2.1 Material selection

Considering the potential application of SOFCs for electric aviation, there arises a necessity to investigate high temperature heat exchanger capable of accommodating temperatures up to 1000 K for waste heat recovery.

Developing materials capable of withstanding extended exposure to high temperatures while maintaining their structural integrity is a critical challenge. Such durability is essential to prevent degradation, corrosion, and mechanical weakness that can lead to failures. Material selection for high-temperature heat exchangers (HTHX) involves a blend of mechanical, thermal, and chemical attributes, as well as manufacturability and economic factors [9]. The aviation sector prioritizes weight and shape over cost. Conventional materials like aluminum, steel, and copper lose structural strength at elevated temperatures. Still, metals are favored for HTHX due to their thermomechanical properties and ease of manufacturing.

Iron-based steels such as SS316 and SS347 offer good mechanical properties up to 550°C and 600°C respectively, though their corrosion resistance is limited. Nickel-based superalloys, like Inconel, provide strength and corrosion resistance at high temperatures. Metal alloys such as Inconel 740H, Haynes 282, and Inconel 625 are viable options for temperatures up to 816°C [9]. Metallic heat exchangers benefit from established correlations for heat transfer and pressure drop needed during the preliminary design of heat exchangers.

However, they lose strength at higher temperatures, as shown in FIG 2. Ceramics offer exceptional high strength, temperature and corrosion resistance for very high-temperature HTHX applications [10]. Ceramic matrix composites (CMCs) like carbon/silicon carbide combine ceramic fibers and a matrix for improved toughness. Challenges in ceramic manufacturing and mechanical joining persist due to brittleness. In addition, correlations for ceramic-based HTHX regarding heat transfer and pressure drop are lacking [11, 12]. Thus, due to its exceptional corrosion resistance, established track record in aviation applications, and its capacity to withstand high temperatures, Inconel 625 is chosen as the material for the HTHX to reject waste heat from a SOFC system.

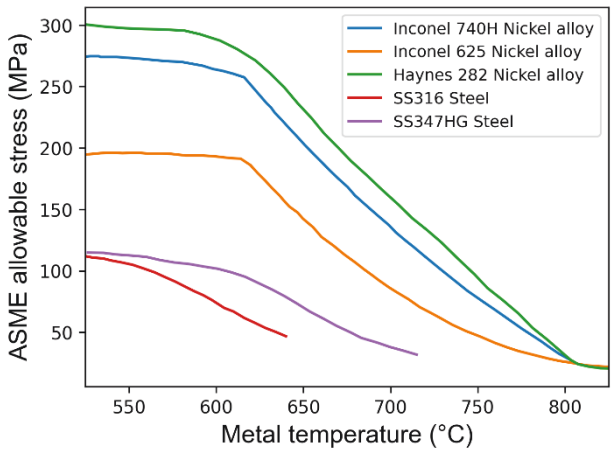

FIG 2. Strength losses of metallic alloys at higher temperature based on Brun et al. and Chordia et al. [13, 14].

2.2 Heat exchanger selection based on the type selection

Highly compact heat exchanger is needed for the aviation sector which are characterized by a large heat transfer surface area per unit volume of the exchanger, resulting in reduced space, weight, support structure and footprint. A heat exchanger is considered to be compact if it incorporates a heat transfer surface that has a surface area density greater than about 700 m^2/m^3 or a hydraulic diameter $D_h \leq 6\,mm$ for operating in a gas stream [15]. Another important consideration in compact heat exchanger design is to minimize the pressure drop across the heat exchanger. A large pressure drop will adversely increase the power offtake, mass and volume at the system level as in addition to the heat exchanger, the size of the compressor at the air side and pump at liquid side will also increase to overcome the pressure loss and to maintain the required mass flow rate. Furthermore, the heat exchanger's lifetime, reliability, and safety aspects must be carefully evaluated to ensure prolonged operation without compromising aircraft safety [16].

Different types of compact heat exchangers are available in literature such as plate, tubular, extended surfaces etc. [10, 15]. Simple plate heat exchangers as shown in FIG 3 are a viable option for high-temperature aviation heat exchanger due to the compact design, efficient heat transfer capabilities, and adaptability to stringent space constraints. The corrugated plate configuration enhances heat transfer rates, while their modular nature facilitates system integration. However, PHEs should be cautiously evaluated in terms of material compatibility, considering their limited resistance to extreme temperatures and potential thermal stress under high-temperature aviation conditions [10, 15, 17]. Another specific type of plate heat exchanger is the printed circuit heat exchanger [10, 15], which offers advantages such as high strength, pressure containment capabilities, and excellent heat transfer performance. Printed circuit heat exchangers eliminate the risks of leakage and corrosion, ensuring long-term reliability. They also offer flexibility in terms of fluid types and flow configurations. However, they are associated with a high pressure drop, which must be carefully considered in the design process [10, 15, 17].

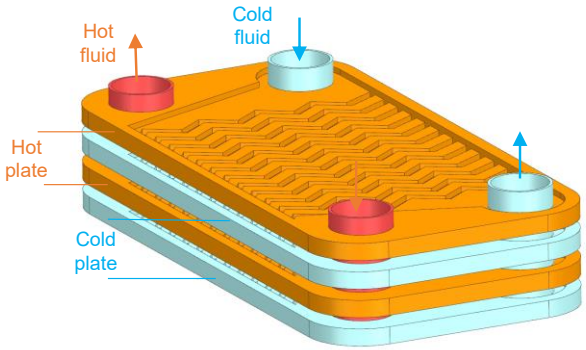

FIG 3. Plate heat exchanger

Extended surfaces fin heat exchangers have been widely used in the aviation industry for their high compactness ratio and efficient heat transfer performance [15]. Plate fin heat exchangers as illustrated in FIG 5 offer a high surface area to volume ratio, allowing for space-efficient installations and effective heat transfer through the use of fins. However, they operate at lower pressures. In contrast, tube fin heat exchangers shown FIG 4 excel in high-pressure applications and are commonly employed when one fluid stream operates at a higher pressure than the other. They offer heat transfer enhancement through the use of fins and can accommodate higher pressure ranges. Due to the higher compactness of the plate fin heat exchanger than the tube fin, plate fins are usually preferred. Thus, due to available correlations, compactness and enhancement of heat transfer coefficient, plate fin heat exchanger is selected for the preliminary design in this study.

2.2.1 Fins selection

Extended surfaces, or fins, in heat exchangers enhance heat transfer by increasing surface area, promoting efficient thermal exchange between fluids. Fins optimize convective heat transfer, reducing thermal resistance and improving overall system performance. This design approach is crucial for maximizing heat transfer rates while minimizing size and material requirements. Different fins geometries are available in the literature such as offset strip fin, louver fin, wavy fin, pin and plain fin.

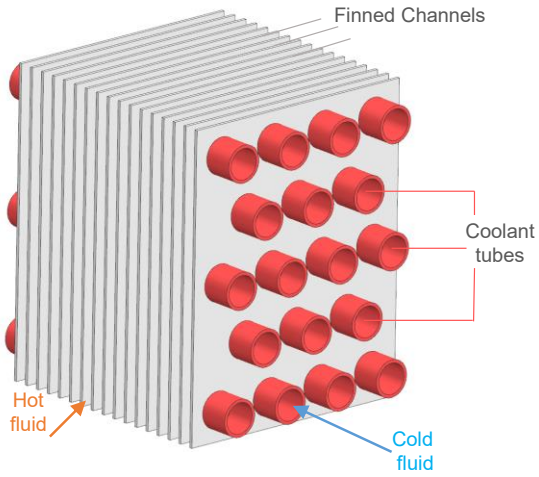

FIG 4. Tube fin heat exchanger

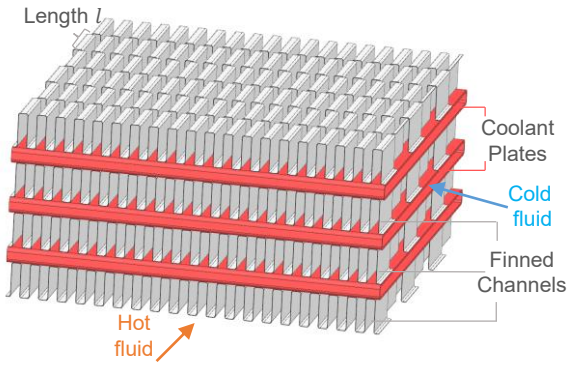

FIG 5. Plate fin heat exchanger

Qasem and Zubair [18], reviewed the thermal-hydraulic performance correlations to evaluate heat transfer rate and pressure drop for the air side of compact heat exchanger. The author concluded that the offset strip fin is an optimal

air side arrangement when the heat transfer, friction power and compactness are the critical criteria for the compact heat exchanger selection. This is shown in FIG 6. Offset strip fins introduce an intricate geometry that disrupts the boundary layer, intensifying fluid mixing and inducing enhanced heat dissipation [19, 20]. The geometry is characterized by the pitch of the fin p_f, height of the fin h_f, thickness of the fin t and length of the fin l, which are shown in FIG 5 and FIG 7 respectively. In conclusion, the utilization of offset strip fins in aviation applications is favored over other fins geometries given in FIG 6 due to their superior heat transfer efficiency, reduced aerodynamic drag, friction power, making them an optimal choice for optimizing thermal management systems in aviation.

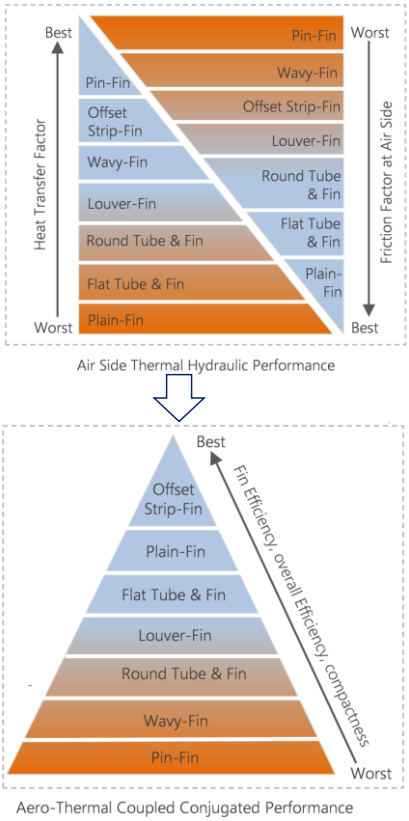

FIG 6. Extended surfaces comparison based on Qasem and Zubair [18] and Sain et al. [21].

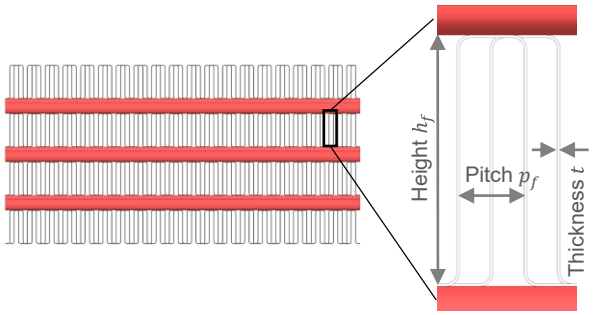

FIG 7. Offset strip fin geometry.

2.3 Thermal boundary conditions

Thermal boundary conditions play a pivotal role in accurately predicting and modelling the performance of fins in heat exchangers. These conditions, encompassing factors such as heat transfer coefficients, fluid properties, and environmental influences, fundamentally dictate the distribution of heat across the fin surface. Precise representation of these conditions is crucial for developing robust heat exchanger correlations, as deviations can lead to inaccuracies in temperature profiles, heat dissipation rates, and overall system efficiency. Also, due to the smaller hydraulic diameter in compact heat exchangers, the flow is usually laminar, and the heat transfer rate in laminar flow is highly sensitive to the thermal boundary conditions. A systematic classification is given by Shah and Sekulic [15].

- T thermal boundary condition: The T thermal boundary condition signifies a uniform wall temperature maintained axially and peripherally throughout the passage length. It is commonly approximated in applications such as condensers, evaporators, and high-liquid-flow liquid-to-gas heat exchangers.
- H1 thermal boundary condition: The H1 condition pertains to a consistent wall heat transfer rate in the axial direction combined with uniform wall temperature across peripheral cross sections. It is applicable to highly conductive materials featuring minimal peripheral temperature gradients, most of them being metals.
- H2 thermal boundary condition: The H2 condition entails a steady wall heat transfer rate both axially and peripherally. It is relevant to poorly conducting materials such as ceramics, plastic with significant peripheral temperature variations.

The Nusselt number (Nu) comparison between the boundary conditions can be done. Generally, $Nu_{H1} > Nu_T, Nu_{H1} \geq Nu_{H2}$, and $Nu_{H2} \cong Nu_T$. For metallic heat exchanger made of Inconel 625 with an offset plate fin configuration, the heat transfer correlations would be based on the H1 thermal boundary condition.

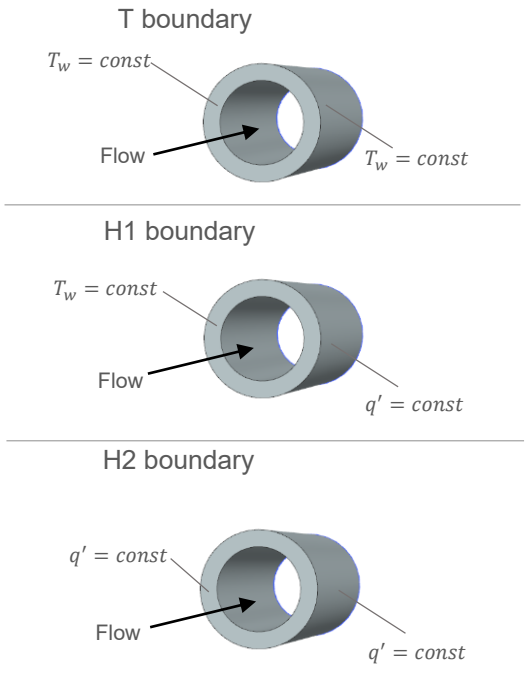

FIG 8. Thermal boundary conditions based on Shah and London [15].

2.4 Heat exchanger thermal and hydraulic performance

For the design approach in this paper, the $\varepsilon - NTU$ method

is used which is most widely used approach in heat exchanger design for calculating the heat transfer and fluid flow performance based on the effectiveness ε and the number of transfer units NTU [5, 15]. A plate fin heat exchanger, with counter flow configuration would require the coolant or hot fluid inlet, outlet ports at same frontal sections as that of the air side. This would adversely increase the flow blockage of the air stream, increasing the pressure loss. On the other hand, a cross flow, as shown in FIG 5 is suitable based on thermal performance and, the $\varepsilon - NTU$ method is easier to implement for cross flow heat exchangers over Logarithmic Mean Temperature Difference (LMTD) and p-NTU methods. In the, $\varepsilon - NTU$ method, the flow from the hot fluid to the cold fluids in the heat exchanger is expressed as given in equation 1.

$$(1)\quad q = \varepsilon \cdot C_{min} \cdot (T_{h,i} - T_{c,i}) = C_h \cdot (T_{h,i} - T_{h,o}) = C_c \cdot (T_{c,o} - T_{c,i})$$

$$(2)\quad \varepsilon = \phi(NTU, C^*, flow\ arrangement)$$

$$(3)\quad C^* = {C_{min}}/{C_{max}}$$

$$(4)\quad \varepsilon = 1 - \exp\left[{\exp(-C^* \cdot NTU^{0.78}) - 1}/{C^* \cdot NTU^{-0.22}}\right]$$

Where, ε is the heat exchanger effectiveness or thermal efficiency. C_{min} is the minimum of C_h and C_c. The heat exchanger effectiveness is a non -dimensional term and it depends on the number of transfer units NTU, the heat capacity rate ratio C^*, and the flow arrangement as given in equation (2). For cross flow heat exchangers, different equations are available to characterize the $\varepsilon - NTU$ based on whether the hot and cold streams are mixed or unmixed. For plate fin heat exchanger, the flow stream consists of separate, parallel flow channels confined by physical boundaries. Thus, the streams are unmixed. The empirical formula given by Digiovanni and Webb [22] is the most common for a single-pass cross-flow heat exchanger with unmixed fluids. The $\varepsilon - NTU$ equation is given by equation (4) and illustrated in FIG 9.

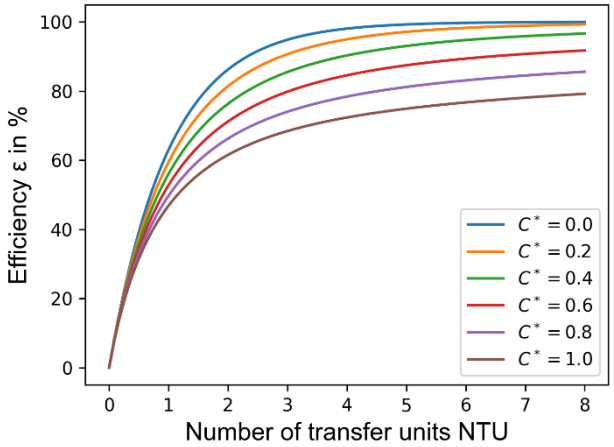

FIG 9. Cross flow heat exchanger $\varepsilon - NTU$ equation for unmixed fluids based on Digiovanni and Webb [22].

The overall heat transfer coefficient (U) and heat transfer areas are calculated based on equation (5) and equation (6). Here, the conduction resistance is neglected due to the small value of thermal conductivity of Inconel 625. In addition, the fouling resistances are neglected for the preliminary design.

$$(5)\quad NTU = {U \cdot A}/{C_{min}}$$

$$(6)\quad {1}/{UA} = {1}/{(\eta_h \cdot A_h \cdot h_h)} + {1}/{(\eta_c \cdot A_c \cdot h_c)}$$

In general, heat transfer performance is measured as Colburn factor, (j), and aero performance in terms of friction Fanning factor (f) quantifying total pressure drop at gas side as combination of viscous and inertial. The most comprehensive correlations for Colburn (j) and Fanning friction (f) factors for the offset strip fin geometry are provided by Manglik and Bergles [23] are given in equation (7) and equation (8) respectively. The hydraulic diameter of the fins is given by equation (9). Here in equation $s = p_f - t, h' = h_f - t$ and $h_f = b_1$. The equations are valid for $120 \leq Re \leq 10^4$ and $0.5 < Pr < 15$. The correlations given are based on H1 thermal boundary conditions.

$$(7)\quad j = 0.65Re^{-0.54}\left(\frac{s}{h'}\right)^{-0.15}\left(\frac{t}{l}\right)^{0.15}\left(\frac{t}{s}\right)^{-0.07} \times \left[1 + 5.27 \times 10^{-5}Re^{1.3}\left(\frac{s}{h'}\right)^{-0.50}\left(\frac{t}{l}\right)^{0.46}\left(\frac{t}{s}\right)^{-1.05}\right]^{0.1}$$

$$(8)\quad f = 9.62Re^{-0.74}\left(\frac{s}{h'}\right)^{-0.19}\left(\frac{t}{l}\right)^{0.31}\left(\frac{t}{s}\right)^{-0.27} \times \left[1 + 7.67 \times 10^{-8}Re^{4.43}\left(\frac{s}{h'}\right)^{-0.92}\left(\frac{t}{l}\right)^{3.78}\left(\frac{t}{s}\right)^{0.24}\right]^{0.1}$$

$$(9)\quad D_h = {(4 \cdot s \cdot h' \cdot l)}/{(2(s \cdot l + h' \cdot l + h' \cdot t) + s \cdot t)}$$

Based on the Colburn factor and friction Fanning factor, heat transfer coefficient (h) and pressure drop (ΔP) for the offset strip fins can be calculated by equation (10) and equation (11) respectively. For the pressure drop calculation (ΔP), only the core frictional pressure drop is considered as it is the major contribution in the total core pressure drop [15]. In equation (10) and equation (11), $G = \dot{m}/A_o$ is the core mass velocity which couple the heat transfer coefficient and pressure drop equation.

For the heat transfer areas of the offset strip fins, the formulas are taken from Shah and Sekulic [15]. There are two types of surface areas primary and secondary heat transfer areas. The primary heat transfer area of offset strip fins is the surface area directly in contact with the fluid or medium from which heat is being transferred. The secondary heat transfer area refers to the additional surface area created by the offset arrangement of the fins, which enhances heat transfer and increasing the convective heat transfer coefficient. Consider the heat transfer areas on the unit cell, the primary surface area $(A_{p,cell})$ and secondary surface area $(A_{f,cell})$ is given by equation (12) and equation (13) respectively. The total surface area of the unit cell $(A_{,cell})$ is summation of the primary and secondary areas given by equation (14).

$$(10)\quad h = {j \cdot G \cdot c_p}/{Pr^{\frac{2}{3}}}$$

$$(11)\quad \Delta P = {(4 \cdot L \cdot f \cdot G_a^2)}/{(2 \cdot g_c \cdot \rho \cdot D_h)}$$

$$(12)\quad A_{p,cell} = 2 \cdot s \cdot l$$

$$(13)\quad A_{f,cell} = 2 \cdot h'l + 2 \cdot h' \cdot t + s \cdot t$$

$$(14)\quad A_{,cell} = 2 \cdot h' \cdot l + 2 \cdot h' \cdot t + s \cdot t + 2 \cdot s \cdot l$$

$$(15)\quad A_{o.cell} = {D_h \cdot A_{cell}}/{4 \cdot l} = s \cdot h'$$

$$(16)\quad \beta = {A_{cell}}/{V_p}$$

The free flow area of an offset strip fin ($A_{o,cell}$) refers to the unobstructed cross-sectional area available for fluid flow through the channels formed between the fins. This free flow area is crucial for determining the pressure drop and fluid velocity within the heat exchanger. For a unit cell it is calculated as provided in equation (15). The compactness (β) is often expressed as the ratio of the effective heat transfer surface area on one side to the volume of the unit cell. It highlights the trade-offs between heat transfer effectiveness and spatial requirements, is given by equation (16).

The assumption made for the fin efficiency of the offset strip fin involves considering uniform heat flow from both sides (plates) and locating the adiabatic plane at the midpoint of the plate spacing. The fin parameter (ml_c) is important for the calculation of fin efficiency which is given by equation (17). The fin efficiency η_f and extended surface efficiency η_o is given by equation (18) and equation (19) respectively.

$$(17)\quad ml_c = \left[2 \cdot {h}/{k_f \cdot t}\left(1 + {t}/{l}\right)\right]^{\frac{1}{2}}\left({b_1}/{2} - t\right)$$

$$(18)\quad \eta_f = {tanh(ml_c)}/{ml_c}$$

$$(19)\quad \eta_o = 1 - \left({A_f}/{A}\right)(1 - \eta_f)$$

2.5 Detailed heat exchanger design

Design approaches for heat exchangers encompass various methodologies, each presenting distinct advantages and limitations. The summary of the design methods is illustrated in FIG 10.

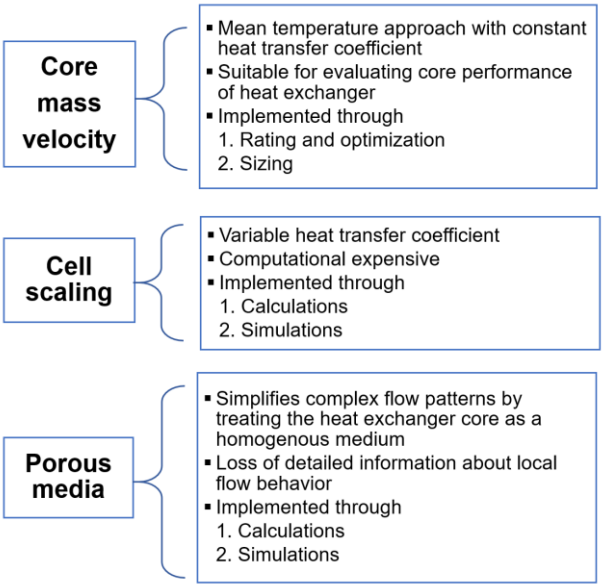

FIG 10. Different types of Heat exchanger design methods.

2.5.1 Core mass velocity approach

The core mass velocity approach presents a pragmatic and expedient methodology for design of plate fin heat exchangers, leveraging its distinctive theoretical foundations and practical advantages. This approach is particularly advantageous during the preliminary design phases, offering rapid estimations of heat transfer performance. It revolves around the characterization of fluid flow within the heat exchanger core, emphasizing the mass flow rate of the working fluid relative to the cross-sectional area of the flow passage. The core mass velocity equation couples the heat duty and hydraulic performance of the heat exchanger. Design of Heat exchanger is based on rating and sizing script. Rating scripts for compact heat exchangers as given in [15] determine the heat transfer rate, outlet temperatures and pressure drop performance based on an existing or an already designed heat exchangers. However, due to the advancements in the optimization algorithms, one can now size a heat exchanger by iterating across the rating script until the required heat flow and pressure drop performance is achieved. Based on this principle, in the current study, the algorithm considers the heat flow and the pressure drop as the constraints which has to be met and it also sets lower and upper bounds on the outer dimensions of the heat exchanger. Moreover, by adding different objectives like volume, mass minimization, one can size a heat exchanger using multi-constraints and multi-objectives which could meet all the requirements from an aviation purpose. Using empirical correlations and design guidelines, rating scripts and optimization methods, yield reasonably accurate results for conventional operating conditions.

The traditional sizing approach given in Shah and Sekulic [15] involves the selection of exchanger construction type, flow arrangement, and the physical size of an exchanger to meet the specified heat transfer and pressure drops within specified constraints. This is implemented using an iterative approach. The coupling of heat transfer and flow friction has been proposed by [5] and used in the sizing methodology given by Shah and Sekulic [15].

$$(20)\quad G = \left[\left({2 \cdot g_c}/{(1/\rho)_m \cdot Pr^{2/3}}\right) \cdot \left({\eta_o \cdot \Delta p}/{ntu}\right)\left({j}/{f}\right)\right]^{1/2}$$

The solution method includes j/f vs Re characteristics for the surfaces on each fluid side. The above equation is useful as the ratio of j/f is a relatively weak function of the Reynolds number for most extended surfaces [5]. Through this, one can readily estimate a fairly accurate value of j/f in the operating range of Re.

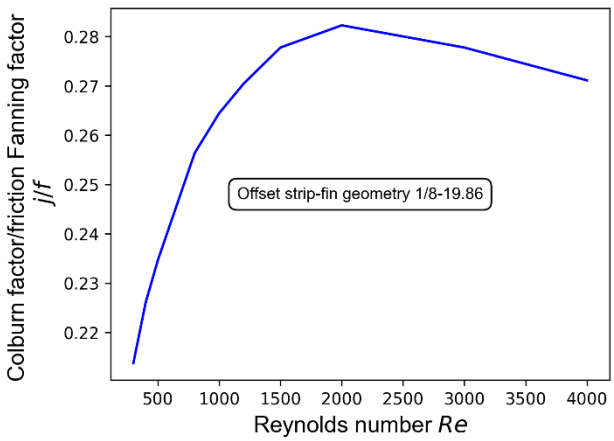

FIG 11. Ratio of Colburn factor to friction Fanning factor (j/f) over Reynolds number (Re) for offset strip fin geometry 1/8-19.86 based on Kays and London [5].

Extended surface efficiency is assumed between 70-90% for a good design. All other parameters in equation (20) can be evaluated based on the problem's specifications. Thus, first approximate value of G can be computed for each fluid

side. Due to the constraints coupling, the iterative solution to the sizing problem converges very fast due to the estimated value of G. However, the sizing problem is limited on number of constraints and objectives it can handle unlike the rating script. Also, it assumes equal heat transfer areas on both sides of the heat exchanger. This can be problematic when designing for gas-liquid heat exchanger. Due to lower heat transfer coefficient of the gas as compared to the liquid it can lead to longer dimensions for the gas side contributing to excessive pressure drop. Thus, in this study more emphasis is given on rating and optimization methodology which would help to find the optimum set of core geometries and operating conditions for the problem specification.

TAB 1. Mean temperatures calculation based on maximum heat capacity on hot fluid side for two fluid heat exchangers.

C_{max} = Hot fluid, C_{min} = Cold fluid	
For C^*< 0.5:	
$T_{h,m}$	$= \frac{T_{h,i} + T_{h,o}}{2}$
$T_{c,m}$	$= T_{h,m} - \Delta T_{lm}$
ΔT_{lm}	$= \frac{(T_{h,m} - T_{c,o}) - (T_{h,m} - T_{c,i})}{\ln[(T_{h,m} - T_{c,o}) / (T_{h,m} - T_{c,i})]}$
$C^* \geq$ 0.5:	
$T_{h,m}$	$= \frac{T_{h,i} + T_{h,o}}{2}$
$T_{c,m}$	$= \frac{T_{c,i} + T_{c,o}}{2}$

TAB 2. Mean temperatures calculation based on maximum heat capacity on cold fluid side for two fluid heat exchangers.

C_{max} = Cold fluid, C_{min} = Hot fluid	
For C^*< 0.5:	
$T_{c,m}$	$= \frac{T_{c,i} + T_{c,o}}{2}$
$T_{h,m}$	$= T_{c,m} + \Delta T_{lm}$
ΔT_{lm}	$= \frac{(T_{h,i} - T_{c,m}) - (T_{h,o} - T_{c,m})}{\ln[(T_{h,i} - T_{c,m}) / (T_{h,o} - T_{c,m})]}$
For $C^* \geq$ 0.5:	
$T_{h,m}$	$= \frac{T_{h,i} + T_{h,o}}{2}$
$T_{c,m}$	$= \frac{T_{c,i} + T_{c,o}}{2}$

However, the core mass velocity approach calculates the thermal physical properties at the mean temperatures dependent on the heat capacity ratio of the fluids. This is demonstrated in TAB 1 and TAB 2. This leads to the assumption of uniform temperature distributions, potentially misrepresenting actual flow and heat transfer dynamics and yielding significant inaccuracies when temperature distributions deviate from uniformity. Moreover, the overall heat transfer coefficient remains constant throughout the length.

2.5.2 Cell scaling

Cell scaling [24], on the other hand, delves deeper into flow and heat transfer characteristics, affording insights into individual cell or segment performance and allowing scrutiny of non-uniform flow and heat transfer patterns. The method consists of subdividing the heat transfer area into a finite number of area elements over which the two fluid streams or their branches successively flow in the same or in a different sequence. By this, the entire heat exchanger is represented by a system of interconnected but nonoverlapping modules or cells with individual flow arrangements. Yet, this method's computational demands render it impractical for initial design estimations, and it hinges on the assumption of scalability and uniform behavior among individual cells.

2.5.3 Porous media

The porous media approach [25], while computationally efficient, is particularly suited for the analysis of intricate internal flow distributions. By simplifying the heat exchanger as a porous medium, computational burden is diminished. This approach proves advantageous when explicit modeling of complex or elusive internal flow distributions, such as secondary flows, presents challenges. However, it presumes homogeneity within the porous material, and while suitable for cases where detailed flow and heat transfer distributions are not the primary concern, it introduces certain simplifications and limitations when compared to more comprehensive computational fluid dynamics (CFD) simulations.

In conclusion, these design approaches for heat exchangers offer a spectrum of advantages and constraints, necessitating careful consideration in alignment with specific design objectives and computational capabilities. In the current study, core mass velocity approach is chosen based on its rapid estimation of heat exchanger performance of heat flow and pressure drop. Moreover, emphasis is given on rating and optimization approach for designing the offset strip fin heat exchanger.

2.6 Optimization algorithm selection

Different algorithms are available in the literature for solving multi objective optimization with constraints. Of them, genetic algorithms, simulated annealing and pattern search methods are common [26]. Genetic algorithms (GAs) offer distinct advantages over simulated annealing and pattern search methods in optimizing complex systems like heat exchangers. GAs excel in exploring large solution spaces by emulating the principles of natural selection, enabling them to discover optimal or near-optimal solutions efficiently. Unlike simulated annealing, which relies on stochastic processes to escape local optima, GAs maintain diverse populations, increasing the likelihood of finding global optima [27, 28].

Furthermore, GAs are particularly effective for non-linear, multi-modal, and discrete optimization problems, which are prevalent in heat exchanger design. While pattern search methods may struggle with high-dimensionality, GAs naturally handle such challenges by evolving solutions over generations. Additionally, GAs is adaptable, requiring minimal problem-specific tuning, unlike simulated annealing, which demands careful parameter adjustment.

The population-based nature of GAs enables simultaneous exploration and exploitation, enhancing convergence speed. In contrast, simulated annealing's single-solution focus and pattern search's limited exploration may lead to slow convergence and suboptimal results. Overall, GAs stand as a powerful optimization technique [26–28] for

intricate heat exchanger design, providing robustness, scalability, and efficiency, particularly in the context of aerospace thermal management.

2.6.1 NSGA-III

Non-dominated sorting genetic algorithm III (NSGA-III) is an advanced and efficient optimization technique designed for solving complex multi-objective optimization problems with multiple constraints. This can be explained through equation (21) where the algorithm can have M number of minimization objectives ($\boldsymbol{f}(\boldsymbol{x})$) subjected to constraints like $\boldsymbol{g}(\boldsymbol{x}), \boldsymbol{h}(\boldsymbol{x})$ etc. The algorithm can also take upper and lower bounds on the variables $\boldsymbol{x_i}$ ($\boldsymbol{i} = \boldsymbol{1}, \boldsymbol{2}, \ldots \boldsymbol{n}.$) where, n is the number of variables. NSGA-III is a descendant of genetic algorithms, tailored to address the challenges posed by problems involving conflicting objectives and constraints. This algorithm demonstrates several advantageous characteristics that make it a compelling choice over other genetic algorithm variants for tackling such intricate optimization scenarios. These are given in the following paragraphs.

(21)
$$\begin{aligned} &\text{Minimize } \left(f_1(x), f_2(x), \ldots\ldots, f_M(x)\right), \\ &\text{Subject to } g_j \;\geq\; 0, j = 1,2, \ldots\ldots, J \\ &\qquad\qquad h_k \;=\; 0, k = 1,2, \ldots\ldots, K, \\ &\qquad\qquad x_i^{(L)} \leq\; x_i \leq x_i^{(U)}, i = 1,2, \ldots\ldots, n. \end{aligned}$$

- **Multi-objective and multi-constraint optimization:**

NSGA-III excels in handling optimization problems with multiple conflicting objectives and constraints. In the context of multi-objective optimization, NSGA-III aims to identify a set of Pareto-optimal solutions, representing the trade-offs between different objectives. Simultaneously, it efficiently manages multiple constraints, ensuring that the generated solutions satisfy the given constraints. This makes NSGA-III well-suited for real-world problems where decisions must satisfy various criteria while adhering to practical limitations.

- **Diversity preservation and convergence:**

NSGA-III incorporates the concept of non-dominated sorting and crowding distance to maintain a diverse set of solutions along the Pareto front. This mechanism encourages the algorithm to explore the entire Pareto front, ensuring a well-distributed representation of trade-offs solutions. At the same time, NSGA-III employs elitist selection to focus on converging toward optimal solutions. This balance between exploration and exploitation enhances the algorithm's ability to provide a comprehensive solution set.

- **Efficient non-dominated sorting:**

The non-dominated sorting technique employed by NSGA-III efficiently categorizes solutions based on their dominance relationships. This leads to a computationally efficient procedure for ranking solutions and maintaining a Pareto front approximation. The reduced computational burden of non-dominated sorting contributes to NSGA-III's effectiveness in solving complex optimization problems.

- **Elitist selection and archive management:**

NSGA-III implements elitist selection by preserving the best-performing solutions from one generation to the next. This preserves valuable information and promotes convergence toward better solutions. Additionally, NSGA-III maintains an external archive of non-dominated solutions, which aids in maintaining diversity and guiding the evolution process toward superior regions of the solution space.

- **Adaptable population sizing:**

NSGA-III introduces an adaptive population sizing mechanism that dynamically adjusts the population size based on the number of objectives and constraints. This adaptability ensures efficient resource utilization and enhances the algorithm's performance for different problem complexities.

In comparison to other genetic algorithm variants, NSGA-III stands out as a robust and well-balanced optimization approach for multi-objective and multi-constraint optimization problems. Its ability to efficiently manage trade-offs, handle constraints, maintain diversity, and adapt population size contributes to its suitability for real-world applications.

In FIG 12, the working principle of NSGA-III is explained through a chart. Initially, a population size has to be selected. The population size refers to the number of candidate solutions or individuals maintained during each generation of the algorithm. A suitable population size is critical as it affects the algorithm's ability to explore the trade-offs between the different objectives. By choosing an adequately sized population it enhances diversity, aiding in the discovery of a well disturbed set of Pareto-optimal solutions while an excessive large population may lead to computational efficiency.

Individual fitness evaluation entails assessing the performance of each candidate solution across multiple conflicting objectives and constraints and obtaining the superior individuals for the next generations. Selected parent solutions undergo crossover, wherein genetic information is exchanged to generate new offspring. This promotes exploration of the search space and the creation of novel solutions. Subsequently, mutation is applied to perturb the offspring's genetic makeup, introducing additional diversity and aiding in escaping local optima. The fitness of each offspring is evaluated by assessing its performance across the multiple conflicting objectives. Mathematical metrics or objective-specific measures are employed to quantify the solution's quality and its position in the objective space. After this, entire population, consisting of both parents and offspring, is merged. The individuals are then ranked into different non-dominated fronts based on their Pareto dominance relationships. The fronts are organized by dominance rank, with lower-ranked fronts indicating better solutions. Within each front, individuals are further prioritized using crowding distance, favoring those with greater spacing in the objective space.

TAB 3. Parameters for NSGA-III.

Parameters	**NSGA-III**
Population size	900
Number of generations	250
Offspring population	700
Reference direction	Das-Dennis [29]
Stalling limit	100

Reference directions are a pivotal aspect of leading evolutionary multi-objective optimization algorithms, such as NSGA-III. Their role involves steering the algorithmic search by dispersing solutions throughout the objective space, thereby facilitating efficient and thorough exploration

of various sections of the Pareto front. This promotes a more comprehensive representation of trade-offs between conflicting objectives. Currently, Das Dennis reference points is implemented in the current study. The method strategically position solution across the objective space by disturbing the points uniformly. This enables systematic exploration of diverse Pareto optimal trade-offs and enhances the algorithm's ability to capture the full spectrum of solutions yielding a well approximated Pareto front.

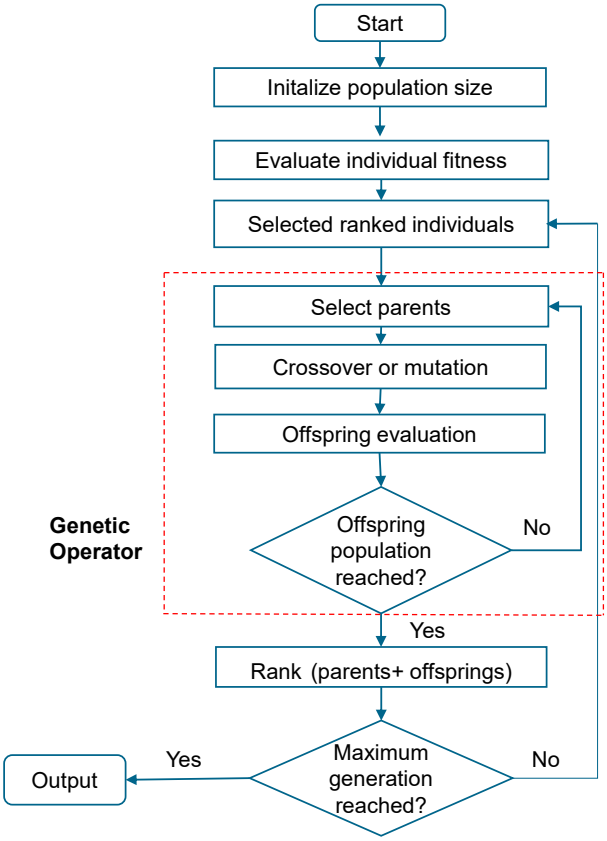

FIG 12. Flow chart of the working principle of NSGA-III.

The stalling limit in NSGA-III acts as a safeguard against getting stuck in one place during the optimization process. It sets a maximum number of attempts the algorithm can make without seeing any significant improvements in the solutions. When this limit is reached, the algorithm takes a smart action to refresh its search. By doing this, the stalling limit prevents the algorithm from becoming unproductive and encourages it to keep exploring different options. This enhances the algorithm's ability to find better solutions, even when progress seems slow, ultimately leading to more effective optimization outcomes.

3 RESULTS

3.1 Design based on core mass velocity and optimization algorithm

In this study, the NSGA-III optimization algorithm is implemented using the pymoo package [6]. For the validation of the NSGA-III optimization, the study uses the example of the sizing methodology provided by Shah and Sekulic [15]. The example is based on the gas-gas single pass crossflow offset strip fin heat exchanger. It contains channels, so called hot side and cold side, through which hot gas and cold gas flows respectively. The example also uses Inconel 625 as the material and it imposes the constraints on the heat transfer and pressure drops at the fluid side. The input parameters are shown in TAB 4. For the fin's geometry, an offset strip fin surface 1/8-19.86 was selected on both the sides of the fluid. The offset strip fins geometries are taken from Kays and London [5] . The heat exchanger fluid used in this example is air for each hot and cold side.

TAB 4. Input parameters based on the example [15].

#	Parameters	Values	Units
1.	Efficiency of heat exchanger ε	83.81	%
2.	Inlet temperature of hot side $T_{h,i}$	1173.2	K
3.	Inlet temperature of cold side $T_{c,i}$	473.2	K
4.	Inlet pressure of hot side $P_{h,i}$	160	kPa
5.	Inlet pressure of cold side $P_{c,i}$	200	kPa
6.	Mass flow rate of hot side $\dot{m}_h$	1.66	kg/s
7.	Mass flow rate of cold side $\dot{m}_c$	2	kg/s
8.	Thermal conductivity of Inconel 625 k_f	18	$W/m \cdot K$
9.	Plate thickness δ	0.5	mm
10.	Pressure drop of hot side ΔP_h	9050	Pa
11.	Pressure drop of cold side ΔP_c	8790	Pa

The optimization algorithm reiterates until the constraints are not solved. Based on the results in TAB 5, it is clear that the deviation between the present study and the reference study was less than 1% indicating very good agreement. The discrepancies in the temperature differentials at both the inlet and the outlet, for both the cold and the hot side, show minimal magnitudes. A similar trend is observed in the pressure drop data for both the hot and cold sides. This consistency underlines the robust agreement between the present study and the reference study. For further optimization of the heat exchanger based on multiple objectives and multi-constraints, same input parameters based on [15] would be used in the following section.

TAB 5. Validation result of the calculation.

	Ref. [15]	Present study	Difference (%)
$\Delta T_h(K)$	585.50	587.08	+0.27
$\Delta T_c\ (K)$	501.80	504.09	+0.45
$\Delta P_h\ (kPa)$	9.05	9.00	-0.55
$\Delta P_c\ (kPa)$	8.75	8.71	-0.45

3.2 Design based on minimized volume

Volume minimization is a critical objective in the preliminary design of heat exchangers for aircraft as it has a profound impact on aircraft efficiency and performance. In addition, minimizing volume helps to optimize the space utilization within the confined aircraft environment, enabling the integration of other vital components. Consequently,

prioritizing volume minimization in the initial heat exchanger design phase directly contributes to the overall effectiveness and competitiveness of aviation systems. In this section, outer dimensions of heat exchanger have been obtained based on the single objective of minimized volume. The constraints for the algorithm remained the same: heat transfer rate and pressure drop at the fluid sides.

The volume of the heat exchanger is calculated based on its outer dimensions as given in equation (22), where L_c and L_h are the external lengths at cold and hot sides respectively and H the total height of the heat exchanger block.

(22) $V = L_c \cdot L_h \cdot H$

The performance constraints for the present study are the total pressure drop in fluid between the inlet and outlet ports of the hot and cold sides; and the ε as thermal efficiency as per equation (4):

(23) $\Delta P_h < 8790\ Pa$

(24) $\Delta P_c < 9050\ Pa$

(25) $\varepsilon > 0.8381$

In addition, heat exchanger configurations are increasingly confronted by spatial limitations that can potentially hinder their operational efficiency. Therefore, geometric constraints are considered within the optimization framework. The spatial constraints are

(26) $0.05\ m < L_c < 1\ m$

(27) $0.05\ m < L_h < 1\ m$

(28) $0.05\ m < H < 2\ m$

To obtain the minimized volume of the heat exchanger, offset fins geometries are taken from Kays and London [5]. These geometries provide us the pitch p_f, height h_f, thickness t and length l of the fin from which heat transfer and pressure drop correlations can be obtained. In addition, the geometries also provide information on the compactness (β) of different fin types and the ratio of fin area to total heat transfer area (α).

TAB 6. Different types of offset strip fins geometries taken from Kays and London [5].

Type	p_f (mm)	h_f (mm)	t (mm)	l (mm)	α	β
1/8-15.2	1.68	10.50	0.152	3.18	0.87	1368
1/8-13.95	1.83	9.53	0.254	3.18	0.84	1250
1/8-15.61	1.63	6.35	0.102	3.18	0.81	1548
1/8-19.86	1.27	2.49	0.102	3.18	0.78	2254
1/9-22.68	1.12	7.65	0.102	2.80	0.88	2069
1/9-25.01	1.02	5.08	0.102	2.80	0.85	2360
1/9-24.12	1.05	1.91	0.102	2.80	0.66	2830
1/10-27.03	0.94	6.38	0.102	2.54	0.89	2466
1/10-19.35	1.31	1.91	0.102	2.54	0.61	2490
1/10-19.74	1.29	1.29	0.051	2.54	0.51	3028
3/32-12.22	2.08	11.20	0.102	2.40	0.86	1115

Thus, for a given application based on heat transfer and pressure drop constraints, the algorithm would indicate which fin geometries should be used in order to achieve the given objective. The fin geometries of Kays and London [5] are manufactured for the experiments.

TAB 7. Minimized volume of heat exchanger obtained.

	NSGA-III	PSO
Volume V (m^3)	0.0614	0.0615
Length at cold side L_c (m)	0.2120	0.2140
Length at hot side L_h (m)	0.1940	0.1934
Height of the stack H (m)	1.4870	1.4970
Fins selected	1/9-24.12	1/9-24.12

To compare the results of the NSGA-III single objective optimization, Particle Swarm Optimization (PSO) is considered [6, 30]. PSO offers efficient exploration of the solution space and rapid convergence, making it ideal for single-objective optimization where a global optimum is sought [26, 30]. Its simplicity and ability to balance exploration and exploitation make it a popular choice for solving complex optimization problems. The working principles of these two optimization techniques are quite different. PSO [30] mimics social behavior by iteratively updating the positions of particles based on their own best performance and the success of their peer, leveraging velocity vectors to explore the solution space. Despite the differences in the working principles, the results for the minimized volume given by these two techniques are almost identical as shown in FIG 13. NSGA-III single objective optimization results. The optimization techniques select the same fin geometry from the lists provided in TAB 6. Although, NSGA-III excels in multi-objective optimization, it can also give very good results even with a single objective and comparable results with another optimization technique preferred for a single objective such as PSO.

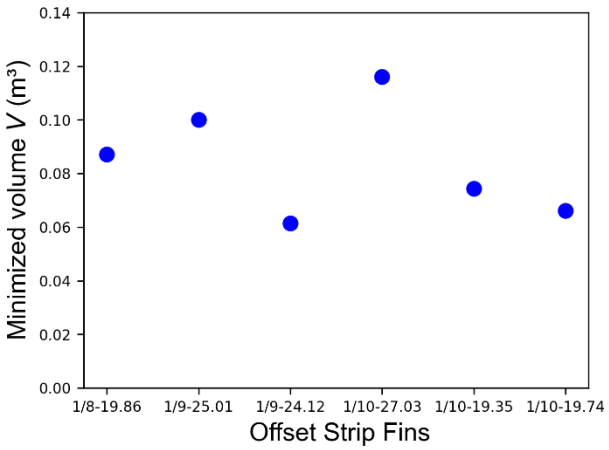

FIG 13. NSGA-III single objective optimization results.

Based on the results obtained for the minimized volume, 1/9-24.12 are the fins selected for both the hot and cold fluid sides. FIG 13 shows the minimized volume obtained for different types of the offset strip fins based on TAB 6. The offset strip fins 1/9-24.12 and 1/10-19.74 showed almost similar volumes for the given application. One of the reasons for the lower volume for the above fin geometries is due to the high compactness of the fins. The fin geometry 1/10-19.74 has a compactness of 3028 which is the highest in the list, due to the small thickness of the fin which is only $0.051\ mm$. The fin geometry 1/9-24.12 has twice the thickness of the 1/10-19.74 geometry with a greater height

and, length of the fin as well. This contributes to more secondary area induced by fins and larger heat transfer areas.

3.3 Design based on minimized volume, mass and frontal areas based on existing fin geometries

In the previous subsection, the optimization was performed based on single objective to minimize volume. Here the best fin geometry (1/9-24.12) was selected based on the list of offset strips given by Kays and London [5]. In this subsection, more objectives are added to the optimization leading multi-objective and multi-constraint problems solving. This would further optimize the heat exchangers geometries and provide a comprehensive perspective, enabling balance competing objective. Through this approach, designers can uncover trade-offs, identify Pareto-optimal solutions, and gain insights into the intricate relationships between design parameters.

To determine the mass of a heat exchanger, it is necessary to combine the mass of the fins on either hot and cold side and the mass of the plates situated between the fins (see FIG 5, FIG 7). The calibration of the fin mass is based on a specific fin design depicted in FIG 7, which shows two offset strip fins. The volume (V_{cell}) and mass (M_{cell}) of each fin are computed using equations (29) and (30), respectively. Furthermore, the total number of fins (n_f) on the cold side can be determined using equation (31). By using the same fin geometry on both fluid sides, the calculated number of fins is actually applicable to both sides. It is important to note that this total number of fins, as described in equation (31), refers to a single fluid passage. In the context of a plate fin heat exchanger, a "passage" signifies a well-defined channel within the heat exchanger structure through which a fluid, typically a gas or liquid, flows. Plate fin heat exchangers are composed of multiple flat plates and fins configured to create a series of alternating narrow passages of the two different fluids with N_p passages for one fluid and $N_p + 1$ passages for the other. The number of passages (N_p) for a plate fin heat exchanger is therefore determined by equation (32).

(29) $V_{cell} = l \cdot t \cdot (p_f + h')$

(30) $M_{cell} = V_{cell} \cdot \rho_{inconel}$

(31) $n_f = \left({}^{L_c}/_{p_f}\right) \cdot \left({}^{L_h}/_{l}\right)$

(32) $N_p = {}^{(H - b_1 - 2\delta)}/_{(b_1 + b_1 + 2\delta)}$

The mass of the fins (M_{fins}) is calculated by multiplying the total number of fins on both the sides by the mass of single cell and the number of passages. Similarly, the mass of the plates (M_{plates}) is calculated using equation (34). Thus, by summing the mass of the plates and fins on both the sides, the mass of the heat exchanger (M_{HEX}) can be obtained. The material used is Inconel 625 and the density is assumed to be constant at $\rho_{inconel} = 8510\ kg/m^3$.

(33) $M_{fins} = 2M_{cell} \cdot n_f \cdot N_p$

(34) $M_{plates} = L_c \cdot L_h \cdot \delta \cdot (2N_p - 1)$

(35) $M_{HEX} = M_{fins} + M_{plates}$

In addition to the volume and mass minimization as a design criterion for compact heat exchangers, minimum frontal area is also an important criterion. A smaller frontal area not only enhances aerodynamics in aircraft, reducing drag and improving fuel efficiency, but also contributes to cost savings through reduced material usage and ensures compliance with spatial constraints.

Moreover, for heat exchangers, minimizing frontal area aligns with the objective of optimizing heat transfer efficiency and is therefore a fundamental consideration. To achieve this, surface designs must be selected that maximize the heat transfer coefficient while meeting specific fluid pumping power constraints. This often results in the choice of heat exchanger configurations with the smallest surface areas, which correlates with the lowest overall volume requirements. Consequently, in gas flow applications, two primary criteria for selecting compact surfaces are emphasized: meeting minimal frontal area (A_{fr}) requirements and minimizing volume usage [15]. To evaluate these criteria, a surface area goodness quality factor, represented as the ratio of the Colburn factor to the friction Fanning factor j/f, is utilized to make design decisions. Using the definitions of j, Nu, f and Re, one can get the ratio j/f can be obtained from [5, 15].

(36) $${}^{j}/_{f} = {}^{Nu \cdot Pr^{-1/3}}/_{f \cdot Re} = \left({}^{1}/_{{A_o}^2 \cdot \eta_o}\right)\left({}^{Pr^{2/3} \cdot ntu \cdot \dot{m}^2}/_{2 \cdot g_c \cdot \rho \cdot \Delta p}\right)$$

The expression enclosed in the parentheses on the right-hand side of equation (36) is solely reliant on the operating parameters and is unaffected by the specific geometry and the heat transfer surface under consideration. Thus, equation can be rearranged as

(37) $$A_o^* = {}^{A_o}\Big/\left[(Pr^{\frac{2}{3}}/2 \cdot g_c \cdot \rho) \cdot (ntu \cdot \frac{\dot{m}^2}{\Delta p})\right]^{1/2} = {}^{1}/_{[\eta_o \cdot (j/f)]^{1/2}}$$

(38) $$A_{fr}^* = {}^{A_{fr}}\Big/\left[(Pr^{\frac{2}{3}}/2 \cdot g_c \cdot \rho) \cdot (ntu \cdot \frac{\dot{m}^2}{\Delta p})\right]^{1/2} = {}^{1}/_{\sigma \cdot [\eta_o \cdot (j/f)]^{1/2}}$$

The dimensionless quantities representing the open flow area and frontal area, denoted as A_o^* and A_{fr}^* respectively, are depicted on the left-hand sides of equation (37) and equation (38). These equations indicate the significance of the parameter j/f, whose relationship with ${A_o}^2$ is inversely proportional under predetermined operating conditions, while keeping η_o constant. A surface characterized by a higher j/f factor is deemed favorable, as it necessitates a diminished free-flow area and consequently a reduced frontal area for the heat exchanger configuration. Therefore, in the current study, three objectives are considered with the minimization of volume, mass and frontal areas. For the minimization of frontal areas, fins are selected which provide the maximum j/f factor.

Different multi objectives and constraints that the optimization are carried out is tabulated in TAB 8.

TAB 8. Different objectives and constraints used in NSGA-III for getting best fin geometries from TAB 6.

NSGA-III multi objectives constraints used		
Number of variables	4	Outer dimensions and fin geometry selection
Number of constraints	3	Pressure drop on both fluid side, heat flow
Number of objectives	4	Volume, mass, frontal areas minimization on both fluid side

In FIG 14, the Pareto front is depicted, which serves as a visual representation of the trade-offs inherent in the optimization of a heat exchanger. Specifically, the optimization aims to minimize both the volume and weight of the heat exchanger. This multi-objective problem involves 11 distinct fin geometries, as originally described by Kays and London. From a thorough analysis, it has been determined that only 4 of these fin geometries are capable of satisfying the prescribed constraints and objectives.

The Pareto front graph allows to draw significant conclusions. First and foremost, it is evident that selecting the fin geometry 1/9-24.12 results in the most favorable outcome in terms of simultaneously minimizing both weight and volume. This geometry stands out as the top-performing choice, achieving a remarkable balance between these two objectives. However, the situation varies for the other fin geometries under consideration. For instance, the second-best option in terms of weight minimization is found in the fin geometry 1/9-25.01. Nonetheless, it is important to note that this particular geometry offers the worst properties for minimum volume. These trade-offs illustrate that, for certain fin geometries, a compromise must be made between the competing objectives of minimizing weight and volume. On the other hand, the fin geometry denoted as 1/8-19.86 exhibits the poorest performance with regard to weight reduction. Despite this, it offers the advantage of occupying less space when compared to the 1/9-25.01 geometry.

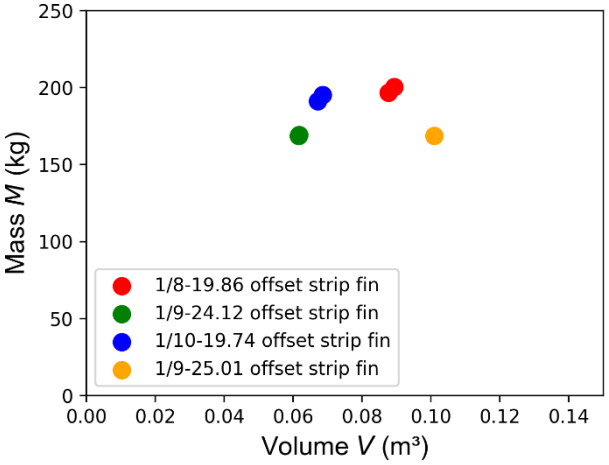

FIG 14. NSGA-III multi objective optimization results for the offset strip plate fin heat exchanger based on minimized volume and mass.

In FIG 15, the Pareto front of the minimized volume and frontal areas of the heat exchanger are shown. The frontal areas of the heat exchanger are calculated by summing up the frontal areas of the cold and hot sides given by equation (37). The Pareto front in FIG 15 reveals the trade-offs between the conflicting objectives.

(39) $$Frontal\ areas = A_{fr_c} + A_{fr_h} = L_h \cdot H + L_c \cdot H$$

As previously noted, selecting the fin geometry 1/9-24.12 results in the smallest volume among all the available solutions. However, this is at the expense of increased frontal area. Conversely, choosing the fin geometry 1/8-19.86, achieves the objective of minimizing frontal areas, resulting in the smallest frontal area values. However, this choice comes at the cost of increasing the volume of the heat exchanger. The critical information to be interpreted from this graph is that reducing the volume of the heat exchanger comes with the trade-offs of increased frontal areas. These trade-offs in turn affect the overall performance of the heat exchanger, as larger frontal areas contribute to increased drag.

The selection between frontal area and volume minimization depends on a complex interplay of factors, including structural integrity, aerodynamic considerations, available space within the aircraft, thermal efficiency requirements, and material limitations. The NSGA-III algorithm is therefore able to perform the optimization based on multi-objectives and constraints and obtain the Pareto front needed for a visual representation of trade-offs between the conflicting objectives. This paves the way for the balanced and well-informed decision making needed at the preliminary design stage.

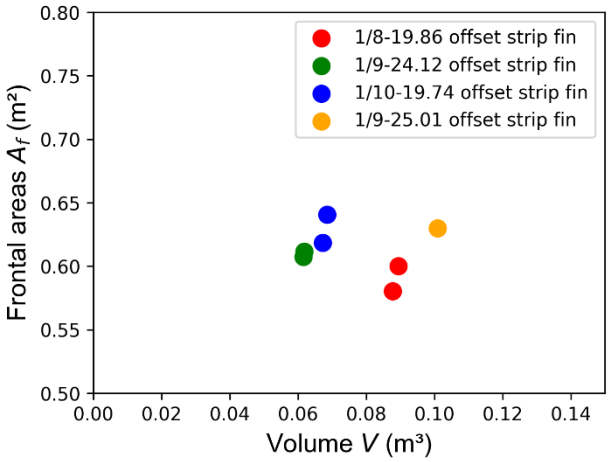

FIG 15. NSGA-III multi objective optimization results for the offset strip plate fin heat exchanger based on minimized volume and frontal areas.

3.4 Design based on minimized volume, mass and frontal areas based on novel fin geometries

In the previous subsections, the offset strip fin geometries were selected from Kays and London [5]. However, with the optimization algorithm can be used to find new fin geometries that can satisfy the heat transfer and pressure drop correlations. Optimization algorithms offer a powerful avenue for advancing the design of novel offset strip fin geometries, particularly in aviation applications. Using these algorithms, engineers can systematically explore an extensive design space to discover innovative fin configurations that optimize heat transfer efficiency, aerodynamic performance, and structural integrity. Tailored to aviation-specific constraints and objectives, the algorithms enable the identification of optimal fin arrangements that minimize mass, reduce drag, and improve cooling efficiency. This process involves iterative refinement of geometries, ultimately resulting in cutting-edge heat exchange solutions that elevate aircraft efficiency, reduce emissions, and extend operational capabilities, thereby exemplifying the transformative impact of optimization techniques in aircraft engineering.

The correlations for the pressure and heat transfer coefficient of the offset strip fins are based on Manglik and Bergles [23]. The correlations impose restrictions on the geometric dimensions of the fins. There are given as below [18, 23].

$$(40)\quad \begin{aligned} 0.134 \leq\ & {}^{s}/_{h'} \leq 1.034 \\ 0.012 \leq\ & {}^{t}/_{l} \leq 0.060 \\ 0.038 \leq\ & {}^{t}/_{s} \leq 0.195 \\ 0.646\ mm \leq\ & D_h \leq 3.414\ mm \end{aligned}$$

The imposed geometric constraints can be incorporated into the NSGA-III optimization algorithm, in addition to the heat transfer and pressure drop constraints. This integration enables the NSGA-III algorithm to yield novel fin geometries that adhere to these defined constraints.

Subsequently, the optimization process was carried out, and the outcomes were compared with those attained in FIG 14. The corresponding Pareto front of minimized mass and volume is illustrated in FIG 16. This graphical representation facilitates a comparative analysis of fin geometry selections. The graphical depiction highlights that the novel fin geometries obtained through Manglik's constraints have lower mass and volume compared to the fin geometries derived from Kays and London. FIG 16, provides a visual representation of the Pareto front, depicting the trade-offs between conflicting objectives associated with fin geometries derived from the Manglik constraints. Within this Pareto front, the fin geometry characterized by the lowest mass has a larger volume compared than to its adjacent solutions. Through this concept of novel fin geometries, a decrease in the volume and mass of the heat exchanger on average by 30% and 35% compared to the fin's geometries taken from the Kays and London has been achieved.

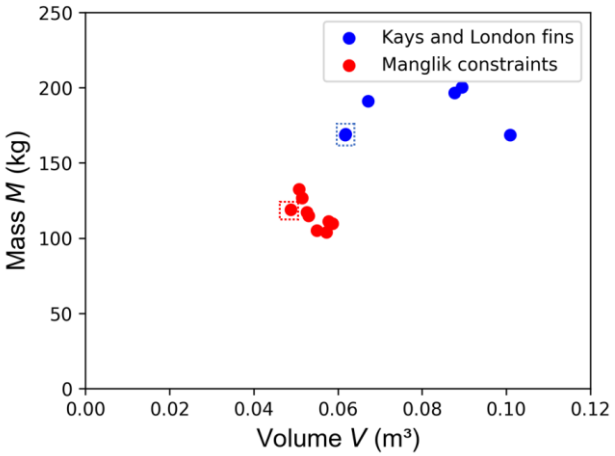

FIG 16. Comparison of novel fin geometries based on Manglik constraints with Kays and London fins for optimized heat exchanger.

Nevertheless, a demonstration is required to understand the differences in the resulting fin dimensions, as detailed in TAB 9. This table shows the results for the dotted red box for the novel geometries from the Manglik [23] constraints and dotted blue box for the geometries from the Kays and London [5] illustrated in FIG 16. The comparison is done on the basis of a minimized volume.

On examination, the novel fin geometry shows that both the pitch and thickness are notably smaller than those of the offset strip fin (1/9-24.12). Conversely, the fin's length is approximately 2 times greater than that of the 1/9-24.12 fin. Consequently, this results in an increased heat transfer area and an improved compactness. These advances consequently contribute to increased volumetric power density and gravimetric power density.

However, despite the enhanced performance demonstrated by the novel fins, it remains imperative to validate these fin geometries through multi-fidelity solutions such as Computational Fluid Dynamics (CFD). This progressive step is essential to further refine the design of offset strip fins as applied in this context. It also remains to be seen whether the fins are manufacturable and durable.

TAB 9. Results comparison between the novel fin geometries obtained by NSGA-III with Kays and London fin (1/9-24.12).

Parameters	**Fins based on Manglik constraints**	**Kays and London fin (1/9-24.12)**
Volumetric power density (MW/m^3)	24	18
Gravimetric power density (kW/kg)	10.09	6.54
Compactness ratio (m^2/m^3)	3400	2830
Heat transfer area on cold side (m^2)	70.40	66.83
Length at cold side $L_c\ (m)$	0.26	0.21
Length at hot side $L_h\ (m)$	0.14	0.18
Height of the stack $H\ (m)$	1.27	1.56
Pitch of the fin $p_f\ (m)$	6.29e-04	1.05e-03
Height of the fin $h_f\ (m)$	2.80e-03	1.91e-03
Thickness of the fin $t\ (m)$	8.5e-05	1.02e-04
Length of the fin $l\ (m)$	6.16e-03	2.80e-03

Considering the application of the heat exchanger in waste heat recovery via Solid Oxide Fuel Cells (SOFC), it is necessary to conduct structural simulations. These simulations are necessary to determine whether the optimized fin geometries can withstand the thermal stresses induced by temperature gradients. Consequently, these analyses are the next steps in the ongoing refinement of the offset strip fin design for the intended application.

3.5 Sensitivity analysis on NSGA-III

The convergence conditions and sensitivity analysis of NSGA-III genetic algorithms are integral aspects of evaluating the algorithm's performance and understanding its behavior in optimization problems. Convergence conditions refer to the criteria that determine when NSGA-III has reached a solution that sufficiently approximates the Pareto front, the set of optimal solutions in multi-objective optimization. Sensitivity analysis, on the other hand, examines the robustness of NSGA-III to changes in its parameters or problem characteristics. This analysis aids in identifying the algorithm's sensitivity to variations and assists in parameter tuning for optimal performance. In this study, parameter sensitivity is understood in terms of its impact on the fitness value.

In the context of optimization through genetic algorithms, achieving consistent results over multiple runs can be challenging due to the inherent probabilistic nature of the algorithm. Conversely, it is possible to establish a specific range within which optimization results can fall by adjusting the algorithm's termination criteria. In the present study, two termination conditions were implemented for the NSGA-III algorithm. First, the optimization was limited to a maximum

of 250 generations. This constraint implies that the optimization process is terminated when 250 generations are reached. Secondly, the termination was initiated after encountering 100 instances of stalling. This has already been explained in the section 2.6.1.

In FIG 17, the convergence history of the NGSA-III algorithm is depicted. The graph shows the progression of the fitness function value over the number of generations. It encompasses two distinct curves: the optimal fitness value and the average fitness value. In this context, the fitness function is defined as the objective function that specifically represents the volume minimization of the heat exchanger.

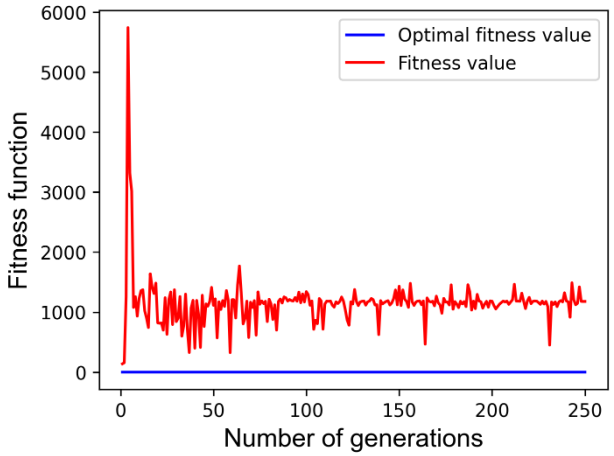

FIG 17. Convergence history of NSGA-III algorithm.

The optimal fitness is the most favorable point reached within the entire genetic space at a given iteration phase. Conversely, the average fitness is the arithmetic mean of all parameter values within the population. Over the course of the computational process, the optimal fitness value displays a steady decrease, indicating that the algorithm is continually improving as it approaches optimal solutions. In contrast, the mean fitness value exhibits fluctuations over the course of the computation. These fluctuations are attributed to the mutation mechanism inherent in the genetic algorithm. This mutation process induces variations in the search point, causing it to gravitate toward a close to the optimal point. Such deliberate perturbations serve to avert the entrapment within local minima and foster a more comprehensive exploration of the solution space. [22]

4 CONCLUSION AND OUTLOOK

This study presents a comprehensive framework for the development of a predictive model aimed at advancing the preliminary design of heat exchangers in the context of electric aviation. Through the integration of optimization algorithms, the design process gains a significant advantage by allowing the systematic exploration of design variables and constraints. This approach holds particular relevance in the realm of Solid Oxide Fuel Cells (SOFCs) for electric aviation, where the exploration of high-temperature heat exchangers capable of accommodating temperatures up to 1000 K is crucial for effective waste heat recovery.

The assessment of materials for high-temperature heat exchangers reveals the superiority of metal-based alloys, particularly Inconel 625, over ceramics due to their favorable heat transfer and pressure drop correlations, as well as ease of manufacturability. The paramount considerations of compactness and minimal pressure drop drive the selection of the plate fin heat exchanger, aided by offset strip fins that effectively augment heat transfer in gas cooling applications.

Furthermore, the application of the NSGA-III optimization algorithm enriches the design process by effectively addressing multiple objectives, constraints, and trade-offs. The validation of the algorithm using textbook examples demonstrates its effectiveness and robustness. The generated Pareto front provides a visual representation of the trade-offs between minimized volume, frontal area and mass, facilitating design choices aligned with specific priorities.

The study extends its scope to introduce novel offset fin geometries, highlighting their improved attributes of compactness, heat transfer area, and power density. However, the need for further validation through multi-fidelity CFD and structural simulations is acknowledged, particularly in high temperature scenarios. As the optimization algorithm continues to pave the way for advanced heat exchanger design, the capabilities of the model could be extended to encompass reliability and safety considerations.

It is worth noting that while the core mass velocity approach has advantages, its assumption of a constant heat transfer coefficient for large temperature differences warrants careful consideration, particularly in cases such as SOFCs. As heat exchanger designs evolve, it becomes imperative to consider temperature dependent correlations for pressure drop and heat transfer. In the pursuit of comprehensive heat exchanger design, future enhancements could encompass reliability, fouling, vibration, safety, and other pertinent design aspects. Ultimately, this study's integration of predictive modelling and optimization algorithms propels the development of innovative, efficient, and optimized heat exchangers for the evolving landscape of electric aircraft.

ACKNOWLEDGEMENTS

We wish to acknowledge Chetan Sain, Antje Link and Dr.-Ing. Robin Brakmann for fruitful insights and interesting discussions, which vastly helped to improve the results presented in this paper.

NOMENCLATURE

Abbreviations

$ASME$	: American society of mechanical engineers
A_p	: Primary heat transfer area (m^2)
A_f	: Secondary heat transfer area by fins (m^2)
A	: Total heat transfer area (m^2)
A_{fr}	: Frontal area (m^2)
A_o	: Free flow area (m^2)
C^*	: Heat capacity ratio
C	: Heat capacity $(J \cdot K^{-1})$
c_p	: Specific heat capacity $(J \cdot K^{-1} \cdot kg^{-1})$
CFD	: Computational fluid dynamics
D_h	: Hydraulic diameter (m)
f	: Fanning friction factor
G	: Core mass velocity $(kg/m^2 \cdot s)$

g_c : Proportionality constant in Newton's second law of motion, g_c=1 and dimensionless in SI units
h : Heat transfer coefficient $(W/m^2 \cdot K)$
h_f : Height of the fin (m)
H : Height of the stack (m)
$HTHX$: High temperature heat exchanger
j : Colburn factor
k_f : Thermal conductivity of the solid $(W/m \cdot K)$
l : Length of the fin (m)
L_c : Length on the cold side (m)
L_h : Length on the hot side (m)
$\dot{m}$: Mass flow rate of the fluid (kg/s)
M : Mass of the heat exchanger (kg)
ml_c : Fin parameter for the efficiency calculation
n_f : Number of fins on fluid side
N_p : Number of passages in the heat exchanger
$NSGA$: Non-dominated sorting genetic algorithm
NTU : Number of transfer units
ntu : Number of transfer units on fluid side
Nu : Nusselt number
Δp : Pressure drop (Pa)
P : Pressure of the fluid
p_f : Pitch of the offset strip fin (m)
PHE : Plate heat exchanger
Pr : Prandtl number
q : Heat transfer rate (MW)
Re : Reynolds number
$SOFC$: Solid oxide fuel cell
t : Thickness of the offset strip fin (m)
ΔT : Temperature difference of the fluid
T : Temperature of the fluid
U : Overall heat transfer coefficient $(W/m^2 \cdot K)$
V : Volume of the heat exchanger (m^3)

Greek symbols

α : Ratio of fin area to the unit cell area
β : Compactness (m^2/m^3)
δ : Plate thickness (m)
ε : Efficiency of the heat exchanger
η : Efficiency of the fin
η_o : Extended surface efficiency
μ : Dynamic viscosity $(Pa \cdot s)$
ρ : Density (kg/m^3)
σ : Ratio of free flow area to frontal areas

Indices

$*_c$: Cold side
$*_{cell}$: Cell
$*_{fins}$: Fins
$*_{HEX}$: Heat exchanger
$*_h$: Hot side
$*_i$: Inlet
$*_{lm}$: Logarithmic mean
$*_m$: Mean value
$*_{max}$: Maximum
$*_{min}$: Minimum
$*_o$: Outlet
$*_p$: Passage
$*_{plates}$: Plates

REFERENCES

[1] *Air Transport Action Group, Waypoint2050, [online], www.atag.org*, Sep. 2020.

[2] *Clean Sky 2 EU, "Clean Sky 2 First Global Assessment 2020: Technology Evaluator Report," May 2021*.

[3] S. Kazula, S. de Graaf, and L. Enghardt, "Review of fuel cell technologies and evaluation of their potential and challenges for electrified propulsion systems in commercial aviation," *J. Glob. Power Propuls. Soc.*, vol. 7, pp. 43–57, 2023, doi: 10.33737/jgpps/158036.

[4] S. Kazula, M. Staggat, and S. de Graaf, "Functional and Safety Challenges of Hydrogen Fuel Cell Systems for Application in Electrified Regional Aircraft," *J. Phys.: Conf. Ser.*, vol. 2526, no. 1, p. 12063, 2023, doi: 10.1088/1742-6596/2526/1/012063.

[5] W. M. Kays and A. L. London, *Compact Heat Exchangers (3rd Edition)*: Scientific International, 2018.

[6] J. Blank and K. Deb, "Pymoo: Multi-Objective Optimization in Python," *IEEE Access*, vol. 8, pp. 89497–89509, 2020, doi: 10.1109/ACCESS.2020.2990567.

[7] K. Deb and H. Jain, "An Evolutionary Many-Objective Optimization Algorithm Using Reference-Point-Based Nondominated Sorting Approach, Part I: Solving Problems With Box Constraints," *IEEE Trans. Evol. Computat.*, vol. 18, no. 4, pp. 577–601, 2014, doi: 10.1109/TEVC.2013.2281535.

[8] H. Jain and K. Deb, "An Evolutionary Many-Objective Optimization Algorithm Using Reference-Point Based Nondominated Sorting Approach, Part II: Handling Constraints and Extending to an Adaptive Approach," *IEEE Trans. Evol. Computat.*, vol. 18, no. 4, pp. 602–622, 2014, doi: 10.1109/TEVC.2013.2281534.

[9] X. Zhang *et al.,* "Recent developments in high temperature heat exchangers: a review," *Frontiers in Heat and Mass Transfer*, vol. 11, 2018, doi: 10.5098/hmt.11.18.

[10] Q. Li, G. Flamant, X. Yuan, P. Neveu, and L. Luo, "Compact heat exchangers: A review and future applications for a new generation of high temperature solar receivers," *Renewable and Sustainable Energy Reviews*, vol. 15, no. 9, pp. 4855–4875, 2011, doi: 10.1016/j.rser.2011.07.066.

[11] J. Haunstetter, V. Dreißigacker, and S. Zunft, "Ceramic high temperature plate fin heat exchanger: Experimental investigation under high temperatures and pressures," *Applied Thermal Engineering*, vol. 151, pp. 364–372, 2019, doi: 10.1016/j.applthermaleng.2019.02.015.

[12] P. E. B. de Mello, S. Scuotto, and F. Ortega, and G. Donato, "Heat transfer and pressure drop in a plate and fin ceramic heat exchanger," *In Conference on Experimental Heat Transfer, Fluid Mechanics and Thermodynamics*, 2013 pp. 16-20.

[13] K. Brun, P. Friedman, and R. A. Dennis, *Fundamentals and applications of supercritical carbon dioxide (SCO2) based power cycles*. Oxford: Woodhead Publishing, 2017.

[14] L. Chordia, M. A. Portnoff, and E. Green, “High Temperature Heat Exchanger Design and Fabrication for Systems with Large Pressure Differentials,” Southwest Research Institute, 2017.

[15] R. K. Shah and D. P. Sekulić, *Fundamentals of heat exchanger design*. New York, Chichester: John Wiley & Sons, 2003.

[16] B. Sundén and J. Fu, *Heat transfer in aerospace applications*. Amsterdam: Academic Press, 2016.

[17] B. Zohuri, *Compact heat exchangers*. Cham, Switzerland: Springer, 2017.

[18] N. A. Qasem and S. M. Zubair, “Compact and microchannel heat exchangers: A comprehensive review of air-side friction factor and heat transfer correlations,” *Energy Conversion and Management*, vol. 173, pp. 555–601, 2018, doi: 10.1016/j.enconman.2018.06.104.

[19] M. S. Kim, J. Lee, S. J. Yook, and K. S. Lee, “Correlations and optimization of a heat exchanger with offset-strip fins,” *International Journal of Heat and Mass Transfer*, vol. 54, 9-10, pp. 2073–2079, 2011.

[20] X. Zheng and Z. Qi, “A comprehensive review of offset strip fin and its applications,” *Applied Thermal Engineering*, vol. 139, pp. 61–75, 2018, doi: 10.1016/j.applthermaleng.2018.04.101.

[21] C. K. Sain, J. Hänsel, and S. Kazula, “Conceptual Design of Air and Thermal Management in a Nacelle-Integrated Fuel Cell System for an Electric Regional Aircraft,” in *AIAA AVIATION 2023 Forum*, San Diego, CA and Online, 2023.

[22] M. A. Digiovanni and R. L. Webb, “Uncertainty in Effectiveness-NTU Calculations for Crossflow Heat Exchangers,” *Heat Transfer Engineering*, vol. 10, no. 3, pp. 61–70, 1989, doi: 10.1080/01457638908939709.

[23] R. M. Manglik and A. E. Bergles, “Heat transfer and pressure drop correlations for the rectangular offset strip fin compact heat exchanger,” *Experimental Thermal and Fluid Science*, vol. 10, no. 2, pp. 171–180, 1995, doi: 10.1016/0894-1777(94)00096-Q.

[24] P. Stephan, S. Kabelac, M. Kind, D. Mewes, and K. Schaber, *VDI-Wärmeatlas: Fachlicher Träger VDI-Gesellschaft Verfahrenstechnik und Chemieingenieurwesen / Peter Stephan, Stephan Kabelac, Matthias Kind, Dieter Mewes, Karlheinz Schaber, Thomas Wetzel, Hrsg,* 12th ed. Berlin, Germany: Springer Vieweg, 2019.

[25] X. Li *et al.*, “Design and modeling of a multiscale porous ceramic heat exchanger for high temperature applications with ultrahigh power density,” *International Journal of Heat and Mass Transfer*, vol. 194, p. 122996, 2022, doi: 10.1016/j.ijheatmasstransfer.2022.122996.

[26] G. Venter, “Review of optimization techniques,” Encyclopedia of aerospace engineering, Wiley & Sons, 2010.

[27] H. Afshari, W. Hare, and S. Tesfamariam, “Constrained multi-objective optimization algorithms: Review and comparison with application in reinforced concrete structures,” *Applied Soft Computing*, vol. 83, p. 105631, 2019, doi: 10.1016/j.asoc.2019.105631.

[28] K. Lee, M. Kim, M. Y. Ha, and J. K. Min, “Investigation of heat-exchanger-sizing methods using genetic, pattern search, and simulated annealing algorithms and the effect of entropy generation,” *J Mech Sci Technol*, vol. 32, no. 2, pp. 915–928, 2018, doi: 10.1007/s12206-018-0142-0.

[29] I. Das and J. E. Dennis, “Normal-Boundary Intersection: A New Method for Generating the Pareto Surface in Nonlinear Multicriteria Optimization Problems,” *SIAM J. Optim.*, vol. 8, no. 3, pp. 631–657, 1998, doi: 10.1137/S1052623496307510.

[30] J. Kennedy and R. Eberhart, “Particle swarm optimization,” in *Proceedings of ICNN'95 - International Conference on Neural Networks*, Perth, WA, Australia, 1995, pp. 1942–1948.